Hindawi
Journal of Advanced Transportation
Volume 2023, Article ID 7954346, 23 pages
https://doi.org/10.1155/2023/7954346

Research Article

Safety Comparison of Simple and Spiral Horizontal Curves Based on Side Friction Factor Dynamic Modeling

Asame Sharf Aldeen,[1] Ali Abdi Kordani ,[1] Afshin Fallah,[2] and Seyed Mohsen Hosseinian [1]

[1]*Department of Civil—Transportation Planning, Faculty of Technical and Engineering, Imam Khomeini International University (IKIU), Qazvin, Iran*
[2]*Department of Statistics, Faculty of Basic Sciences, Imam Khomeini International University (IKIU), Qazvin, Iran*

Correspondence should be addressed to Seyed Mohsen Hosseinian; s.m.hosseinian@edu.ikiu.ac.ir

Received 19 October 2022; Revised 31 December 2022; Accepted 24 January 2023; Published 10 February 2023

Academic Editor: Maria Castro

A horizontal curve's geometric design is considered an important factor in highway accidents, and simple and spiral curves are regarded as the most common types of horizontal curves. Various factors affect the safety of horizontal curves, one of the most important of which is the side friction factor in the horizontal curves. Therefore, in this study, the safety of simple and spiral horizontal curves was investigated for the E-class sedan, E-class SUV, and two-axle conventional truck based on the side friction factor. In this regard, CarSim and TruckSim vehicle dynamic simulation software were utilized using 360 scenarios, including vehicle speed, vehicle type, curve radius, and road geometry. It was revealed that the maximum side friction factor for all vehicles in the simple horizontal curve was higher than the spiral horizontal curve. Also, the process of increasing the side friction factor was carried out with a gentler slope in the spiral horizontal curve. Except for the radius of 0.7 times the maximum radius of the spiral horizontal curve (R) for the truck and the radii of 0.7 R and 0.9 R for the sedan and SUV, the maximum side friction factor in simple and spiral horizontal curves was lower than the AASHTO recommended values, which shows that the spiral horizontal curve was better and safer compared to the simple horizontal curve based on the side friction factor.

1. Introduction

After carrying out the design considerations in drawing the variants of a project and choosing the best project line, it is necessary to design horizontal curves at the road breakpoints, the type of which is selected based on the geometric design of the road [1–3]. Road design has undergone many changes over time, and humans have used curves at the collision of paths for purposes such as increasing safety, reducing costs, and shortening paths, one of the most common of which is simple and spiral horizontal curves [4, 5]. When crossing a simple horizontal curve due to the presence of centrifugal forces, a vehicle is pushed to the curve outside, which in addition to the possibility of collision with the vehicle crossing the opposite lane, there is also the possibility of the vehicle overturning [6, 7]. Therefore, to enhance the curve safety, the centrifugal force is controlled by implementing a one-way slope, known as superelevation [8]. In a simple horizontal curve, a part of superelevation is applied in the tangent path, and another part is used in the simple curve, but when the spiral curve is used before and after the horizontal curve, the superelevation in the spiral curve is gradually applied along the spiral section [9–11]. In simple curves, when entering the curve, the lateral acceleration is applied to the vehicle and the passengers at once, while if the superelevation is provided before the curve, the lateral acceleration changes are noticeable at the entrance to the curve, which reduces safety [12, 13]. The AASHTO Green Book has introduced a radius as the application of the maximum radius in spiral curves. In the current study, the safety investigation is considered through the analysis of the application of the maximum radius in the spiral curves. So

far, few studies have been carried out quantitatively on how to relate the spiral curves used in the horizontal curve to the amount of the vehicle's skidding potential. The main issue is actually increasing safety and reducing the rate of accidents due to the application of the maximum radius in a spiral in a horizontal curve. This research aimed to achieve the maximum radius of use of spiral curves with regard to the safety of vehicles based on the side friction factor using vehicle dynamic simulation software and compare it with the maximum radius of spiral use obtained from the AASHTO Green Book.

In conducting this research, the background of the studies conducted around the research subject and their results are first presented. Then, the behavior of vehicles is investigated by vehicle dynamic simulation using CarSim and TruckSim software. In this way, the software inputs include the vehicle type, speed, curve radius, longitudinal slope of the route, superelevation, and cross-section characteristics, and by the use of the results of the software, the side friction factor of vehicles is presented. Finally, the simulation results obtained from the software are presented.

2. Literature

Bonneson presented a series of friction factors using the vehicle-dynamic approach. Based on his research, a sharp horizontal curve located on a downgrade is of great concern because drivers tend to use the brake to maintain a safe speed, and they also like to use the brake further to reduce speed as they get closer to the start of the curve. He pointed out that the side friction factor depends on speed, radius, superelevation rate, vehicle type, and roadway grade. When considering the effects of roadway grade on friction, he mentioned that the AASHTO Green Book generally underestimates side friction demand for most horizontal curves, particularly those with steep grades, little superelevation, and a large radius [14]. Molan and Kordani conducted a study to examine the impact of the combination of longitudinal grades and horizontal curves on the safety factors, including lateral acceleration and side friction, using CarSim and TruckSim simulation software. The stability of different vehicles was also investigated in relation to rollover and skidding. Results illustrated that in the horizontal curve, the most dangerous section for a vehicle was the entrance of the curve because of the changes in the lateral acceleration and the steering angle. Moreover, the influence of braking on vehicles' side friction factor was evaluated. They indicated that braking had remarkable effects on the side friction factor, particularly for sedans. Therefore, braking is an important threat to the safety of truck based on rollover and to the safety of sedan based on skidding. Also, it was indicated that based on AASHTO, the side friction demand is greater on steep upgrades owing to the tractive forces [15]. Kordani et al. conducted a study to indicate the relationship between longitudinal grade and side friction factor in the horizontal curve using three-dimensional simulation models. For this aim, they presented various models to assess these parameters according to vehicle types (sedan, SUV, and truck), longitudinal grade, and design speed. This study involved performing various multi-body simulation models using TruckSim and CarSim, developing regression analysis for acquiring relationships among parameters, and presenting models for side friction factors. It was indicated that the side friction factor is higher than the downgrade for all vehicles while cornering. Results also revealed side friction factor significant differences for a passenger car in comparison with a heavy vehicle [16].

Kordani and Molan studied the safety of combined horizontal curves and longitudinal grades based on vehicle dynamics simulation software. TruckSim and CarSim software were applied in this research to simulate the dynamic behavior of an E-class sedan, an E-class SUV, and a two-axle conventional truck. The outputs of the simulation were the diagrams of lateral acceleration and forces imposed on the vehicle. In this research, two different driving behaviors were considered in the simulation process: in one, the driver negotiates the curve at a constant speed and without braking; in the other, the driver uses brakes while passing downgrades. The first driving type is almost impossible on steep downgrades, where drivers usually need to use the brake to decelerate and control the vehicle's lateral offset. Results indicated that at the constant speed (without braking), the side friction factor increases as the downgrade increases, meaning that more side friction demand is produced on steep downgrades compared with flat grade and mild downgrades. However, the effects of braking on side friction factors was found to be significant. It was also revealed that there is an agreement between the simulation results for SUV and the AASHTO side friction factors [17]. Kordani et al. also examined the impact of simultaneously occurring vertical sag curve and a horizontal curve on lateral accelerations and side friction factors using simulation modeling. This research examined the influence of bilateral curvatures in both vertical and horizontal dimensions of sag curves and their relocations regarding one another using variables like lateral accelerations and side friction factors. Various simulation models were carried out using TruckSim and CarSim at four speeds of 60, 80, 100, and 120 kilometers per hour. Moreover, the diagrams indicating employed forces in all horizontal, vertical, and lateral dimensions were regarded in evaluating each model to calculate the maximum side friction factor. It was revealed that the maximum side friction factor was located where the deepest point on the vertical sag curve was placed in the middle of horizontal curves. Moreover, the side friction factor for the truck was much lower than the SUV and sedan. However, the lateral acceleration of the truck was more than other vehicle types. Thus, it indicated that the skidding potential of SUV and sedan was much more than their rollover potential. Conversely, rollover potential of the truck was much more against the skidding potential in the specified case [18].

Abdi Kordani et al. examined the effects of the shoulder in the horizontal curve on highway safety regarding roll angles. A 324 scenarios were examined in the current study to simulate vehicle dynamics using CarSim and TruckSim simulation software. Also, the impact of shoulder surfaces' materials, shoulder slopes, and shoulder widths on enhancing safety according to the driver's behavior and highway geometry was evaluated using vehicle dynamics

simulations. In this research, according to vehicles' position in the horizontal curve in different shoulder kinds, modeling was conducted for the roll angles of vehicles. This study contained 3D modeling through simulation software, which evaluated the changes in roll angles in various types of vehicle locations on a shoulder against speed changes and presented the multivariate regression model to examine the relationships of factors by statistical methods. The result indicated that shoulder types (cross slope, material, and width) influenced the safety regarding vehicle's roll angles. They also reported that this effect depended on geometric and dynamic specifications and vehicle type [19]. Qu et al. examined the effect of speed and roadway geometry in combined alignments of freeways on the lateral stability of the tractor-semitrailer by using TruckSim vehicle dynamics simulation. The maximum lateral loading transfer ratio and wheel side friction demand was applied to measure the rollover and skidding risks. Also, by the use of statistical analysis, the effects of different parameters on the lateral stability of the tractor-semitrailer were investigated. It was revealed that the speed and radius had a considerable effect on the lateral stability, whereas downgrades had a significant effect. Moreover, the results illustrated that lower safe speed should be employed on wet highway surfaces on a curved downgrade [20]. Abdi conducted dynamic modeling to examine the effect of vertical and horizontal curve combinations on the lateral acceleration and side friction factor. Multiple simulation tests were performed in the present research using TruckSim and CarSim dynamic simulation software. Simulation tests were carried out on various vehicle types of sedan, SUV, and truck. Position (location of horizontal and vertical curves relative to each other), grade, delta, and speed were factors regarded in modeling. It was indicated that the SUV and sedan experienced more side friction compared to the truck at the first and second quarter of vertical curves. The side friction factor was greater in critical situations compared to the AASHTO recommended amounts. The rollover possibility was higher in trucks due to their higher lateral accelerations. The statistical analysis of this study indicated that the positions and grades did not influence SUV and sedan side friction factors, which could be overlooked [21].

Abdollahzadeh Nasiri et al. conducted a study in which the safety aspect of horizontal curves under the AASHTO standard is evaluated. Several factors, including vehicle weight, vehicle dimensions, longitudinal grades, and vehicle speed in the geometric design of curves, were investigated using a multibody dynamic simulation process. According to AASHTO, a combination of simple, circular, and spiral transition curves with various longitudinal upgrades and downgrades was designed. The analysis was based on the side friction between the tire and the pavement and also the safety margin parameter. The results showed that designers must differentiate between light and heavy vehicles, especially in curves with a high radius. Evaluation of longitudinal grade impacts indicated that the safety margin decreases when the vehicle is entering the curve. Safety margin reduction on the spiral curve occurred with a lower grade toward the simple circular curve. Also, by increasing the speed, the difference between side friction demand obtained from simulation and the side friction demand recommended by AASHTO increased [22]. Javadi et al. evaluated the effects of road shoulder specifications in the roadway-shoulder joint in a horizontal curve on dynamic factors affecting vehicle rollover. Moreover, driver behavior and lateral accelerations were examined regarding the effect of shoulder specifications at a curve. The specifications regarded were pavement, transverse slope, and width. The dynamic simulations were applied to conduct this study, and the number of scenarios in the present research was 324. The regression analysis was carried out with the dependent variables of lateral accelerations and rollover rates. The independent variables were various vehicle types (sedan, SUV, and truck), driver behavior, shoulder specifications, and vehicle dynamics. It was indicated that shoulder specifications had a significant effect on the safety based on the lateral accelerations and rollover rates of the vehicles. Represented effects differed among various vehicle types, which were calculated by the structural and dynamic features of vehicles [23]. Moradi et al. presented a new geometric design approach to reduce vehicle speed in any accident-prone downgrade highways using dynamic vehicle modeling. They proposed an approach to correcting the longitudinal profile of roads by replacing the consecutive downgrades and upgrades with a continuous downgrade at two constant speeds of 70 and 100 km/h. They showed that the vehicle speed is reduced by using this method before entering an accident-prone site without the driver's involvement and braking [24].

3. Methodology

In this section, the process of this study is presented. First, the reason for choosing the simulation software used in this research is discussed, then a flowchart is drawn to introduce the research process briefly, and then the details of the calculation and simulation process and how to obtain data for analysis are discussed.

CarSim and TruckSim software were used in this study, which have the ability to receive the desired geometric design of the user widely and are multibody simulation packages developed by the Mechanical Simulation Corporation (MSC). These simulation software programs were employed in the current research due to variations in vehicle types and the necessity of considering dynamic behavior for the safety evaluation of the vehicle motion. Several well-known vehicle manufacturing companies, such as BMW and Ford, as well as the authors of the National Cooperative Highway Research Program report 774, have used CarSim and TruckSim for various vehicle simulating purposes [25]. One of the most important features of these simulation programs is their ability to combine horizontal curves, which include simple and spiral horizontal curves. Also, a complete set of light and heavy vehicles are available in these software programs, which are often available and common vehicles on the roads. The output results of these programs, in addition to the set of charts and graphs, can be presented in the form of animation, which facilitates understanding of the results. Finally, the output results of these simulations can be shown in Excel at different stations along the route. It should

be noted that one of the drawbacks of studies on the design of horizontal curves is that they do not consider the vehicle parameters in the equation of the geometric design. Therefore, the advantage of using the vehicle dynamics simulation method is the effective characteristics of vehicles on the geometric design of the routes, which is considered one of the main objectives of this study, along with the side friction factor.

In this research, by performing 360 simulation tests with the use of CarSim and TruckSim vehicle dynamics simulation software, the application of the maximum radius in the spiral horizontal curve was examined. The flowchart of the brief introduction of the process of conducting this research is indicated in Figure 1.

3.1. Calculations to Draw Simple and Spiral Horizontal Curves. In this section, calculations for obtaining data related to drawing the simple and spiral horizontal curves carried out in this research, including the length of superelevation, spiral curve length, and horizontal curve radius, are presented, the relationships of which are shown in the AASHTO Green Book. Also, the percentage of the studied radii was 130, 110, 100, 90, and 70% of the application of the maximum radius in the spiral curve (R).

3.2. Drawing Paths with a Spiral Curve in Civil 3D Software. Because the simulation software used in this research cannot directly draw the spiral horizontal curve, the Civil 3D software was used, and the path points were taken as $(X.Y)$ from this software. These points were entered into the simulation software, and the path was drawn with the spiral curve. Table 1 shows the path points with the spiral curve as $(X.Y)$ taken from the Civil 3D software.

3.3. Simulation Process. In this section, the details of the simulation carried out in this research, which includes the inputs and outputs of simulation software, are presented.

3.3.1. Vehicle Type. In this research, the vehicles considered in the simulation tests, including two types of passenger cars of E-class Sedan and E-class SUV, and a two-axle conventional truck, were selected, each of which will be explained in the following:

(1) E-Class Sedan. This vehicle was used in simulation tests as a representative of common passenger cars due to its mechanical and geometrical characteristics. Figure 2 and Table 2 specify the picture of the desired vehicle and its geometrical characteristics, respectively. Figure 3 shows the dimensions and mass of E-class Sedan and the distance of the vehicle mass center from the ground and front axle.

(2) E-Class SUV. This vehicle was used in simulation tests as a representative of SUVs due to its mechanical and geometrical characteristics. It should be noted that according to the geometric characteristics of this vehicle, it is expected that the potential of overturning and skidding of this vehicle is more than that of Sedan. Figure 4 shows a picture of E-class SUV, and Table 3 shows the geometrical characteristics of this vehicle. Figure 5 also shows the dimensions and mass of the E-class SUV and the distance of the vehicle's mass center from the ground and front axle.

(3) Two-Axle Truck. This vehicle is used as a representative of cargo vehicles in simulation tests according to its mechanical and geometric characteristics. Figure 6 shows a picture of a two-axle truck, and Table 4 shows the dimensional characteristics of this vehicle. Also, Figures 7 and 8 show the characteristics of the dimensions and mass of the truck vehicle and the distance of the vehicle mass center from the ground and front axle.

3.3.2. Path Geometric Design

(1) Cross-Section. Due to the fact that in the current research, the dynamic simulations of vehicles are performed in different geometric conditions, therefore, the path is one of the most important parameters of the research study, which includes the median and shoulder of the path. For this research study, the median path width was 3.6 m, the maximum path superelevation was 8%, and the normal slope was 2%.

(2) Path Plan and Pavement Conditions. The design of the path plan was considered as follows:

(i) Simple horizontal curves (tangent, circle, and tangent)

(ii) Spiral horizontal curves (tangent, spiral, circle, spiral, and tangent)

Also, in this study, similar to the previous research study [21], the asphalt pavement with dry condition was considered.

3.3.3. Driver Behavior. In the current study, the driver entered the curve without braking and at a constant speed. The design speed of the vehicle was calculated according to the AASHTO Green Book.

3.3.4. Simulation Outputs. The outputs of the simulation software used in this research are presented in Figures 9 and 10, which include the following:

(i) Diagram of the lateral force on the wheels of vehicles (Figure 9)

(ii) Diagram of the vertical force on the wheels of vehicles (Figure 10)

3.3.5. Number of Designed Tests. The flowchart of the test modes presented in this research is shown in Figure 11. According to this figure, there are two modes based on the horizontal curve, three modes based on the vehicle, five

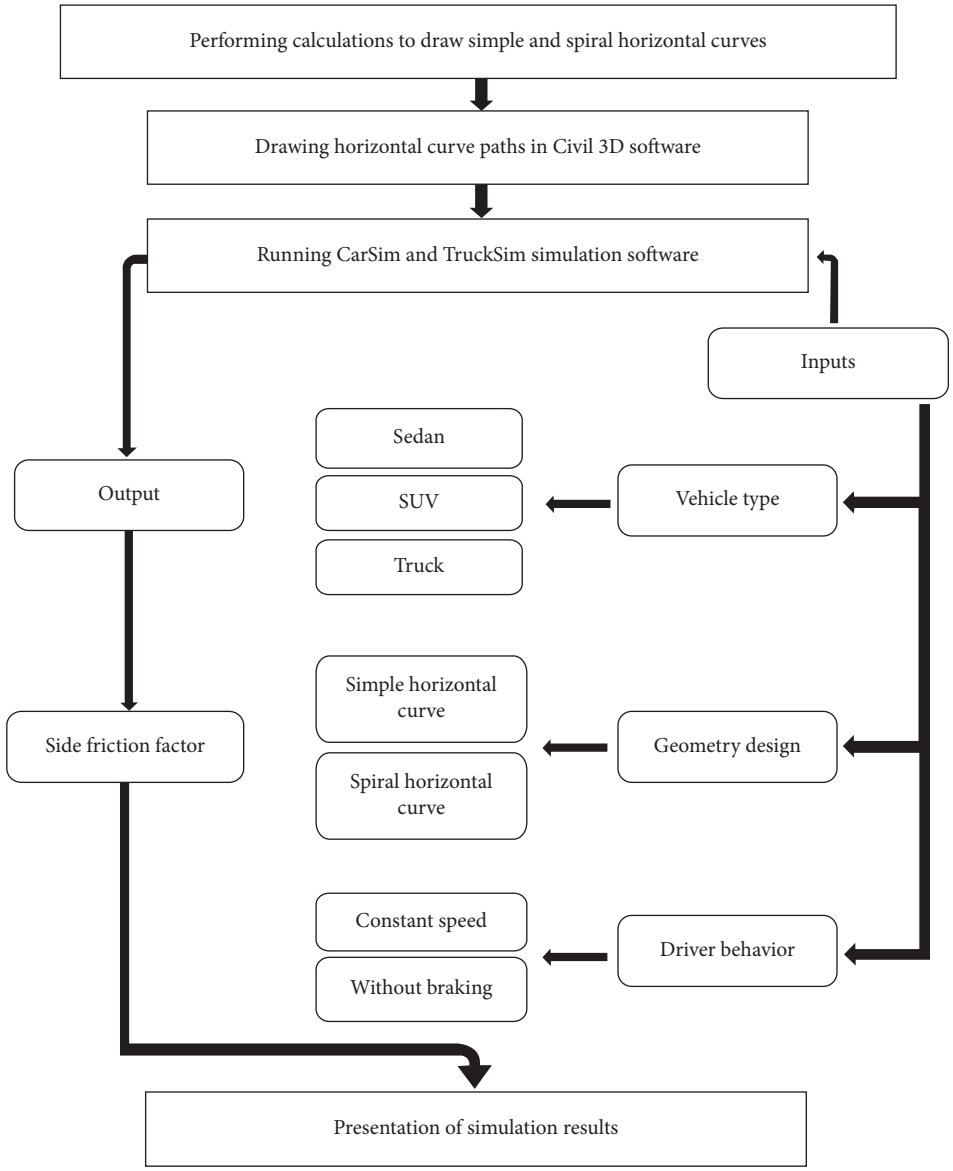

Figure 1: Flowchart introducing the research process.

modes based on the radius of the curve, and twelve modes based on the speed of the vehicle, so the number of presented tests was equal to 360 (2 multiplied by 3 multiplied by 5 is multiplied by 12).

3.4. Calculating the Side Friction Factor. By extracting the output from simulation tests by using the datasets corresponding to lateral and vertical forces on vehicle wheels, equation (1) calculates the side friction factor:

$$f_y = \left|\frac{F_y}{F_z}\right|, \tag{1}$$

where f_y is the side friction factor, F_y illustrates the sum of lateral forces on the wheels of vehicles, and F_z is the sum of the vertical forces on the wheels of vehicles.

4. Results

After completing the data simulation steps, the results obtained from the vehicle dynamics simulation software are presented in this section.

4.1. Side Friction Factor Diagrams for Two-Axle Truck. Since the mass center of vehicles is not exactly in the middle of the axles, the weight distributions on the axles and wheels are not the same. In addition, when rotating in a horizontal curve, due to the application of centrifugal acceleration, this weight distribution on the wheels will change more, and finally, the side friction factor of wheels differs from another wheel, and each axle differs from one another. In this research study, graphs have been drawn for all existing modes, and a separate analysis was carried out. The side friction factor is denoted by f_y and the output results for the two-axle truck are presented.

Table 1: Path points with the spiral curve.

Station	X	Y
0 + 000.00	0	0
0 + 005.00	5	0
0 + 010.00	10	0
0 + 015.00	15	0
0 + 020.00	20	0
0 + 025.00	25	0
0 + 030.00	30	0
0 + 035.00	35	0
0 + 040.00	40	0
0 + 045.00	45	0
0 + 050.00	50	0
0 + 055.00	55	0
0 + 060.00	60	0
0 + 065.00	65	0
0 + 070.00	70	0
0 + 075.00	75	0
0 + 080.00	80	0
0 + 085.00	85	0
0 + 090.00	90	0
0 + 095.00	95	0
0 + 100.00	100	0
0 + 105.00	105	$1.00E-04$
0 + 110.00	110	0.0011
0 + 115.00	115	0.0064
0 + 120.00	120	0.0196
0 + 125.00	124.9999	0.0442
0 + 130.00	129.9997	0.0839
0 + 135.00	134.9994	0.1421
0 + 140.00	139.9987	0.2226
0 + 145.00	144.9976	0.3288
0 + 150.00	149.9958	0.4643
0 + 155.00	154.9929	0.6328
0 + 160.00	159.9887	0.8377
0 + 165.00	164.9827	1.0826
0 + 170.00	169.9744	1.3696
0 + 175.00	174.9636	1.6987
0 + 180.00	179.9497	2.0699
0 + 185.00	184.9326	2.4833
0 + 190.00	189.9118	2.9387
0 + 195.00	194.887	3.4361

Figure 2: E-class sedan.

4.1.1. Side Friction Factor on the Path. The paths examined in this research study include simple and spiral horizontal curves. In the first part of the analysis, the side friction factor along the path is discussed. In this section, due to a large number of investigation modes, the radius of the investigated curve is equal to the maximum radius of the use of spiral, and 100 km/h speed is selected. Before starting the analysis, it is necessary to introduce the path length for the simple and spiral horizontal curves with radius R.

Table 2: Specifications of E-class sedan.

Parameter	Value
Length	4250 mm
Width	1880 mm
Height	1480 mm
Wheels distance	3048 mm
Wheel center height from the ground	375 mm
Mass center height	590 mm
Weight	1653 kg

(i) Path length with the simple horizontal curves: the path includes a tangent, circular curve, and tangent in this section. The first tangent section of the path is from station 0 to station 150 meters, the circular section is from station 150 to station 1080.3 meters, and the last tangent section is from station 1080.3 meters to the end of the path. The superelevation length calculated for this path is equal to 57 meters. The application of this superelevation on the path consists of three stages. In the first stage, it increases from the normal slope at station 104 to the maximum superelevation at station 161. In the next stage, the superelevation is constant from station 161 to station 1069.3 meters, and in the last stage, it decreases from the maximum superelevation at station 1069.3 to the normal slope at station 1126.3 meters.

(ii) Path length with the spiral horizontal curve: the path with the spiral curve includes five sections of the tangent, first spiral, circular curve, last spiral, and tangent. The first tangent continues from station 0 to station 104, the first spiral from station 104 to station 163, the circular part from station 163 to station 1033.92, the last spiral section from station 1033.92 to station 1090.92 and the last tangent section from station 1090.92 until the path ends. The calculated spiral length for this path is equal to 59 meters. In this path, superelevation is applied along the spiral length.

Figure 12 shows the side friction factor in a simple horizontal curve along the path for the truck, where the horizontal axis is the length of the path and the vertical axis is the side friction factor. From the figure, the side friction factor in different sections of the path can be seen, which includes the tangent section, the circular curve, and the next tangent path. This factor is constant in the tangent section from 0 to near the superelevation starting point. Then, it decreases 20 meters in the next section to the point before the circular curve and increases 20 meters before the circular curve. In the circular curve's initial section, the side friction factor continues to increase until the maximum side friction factor, which is 0.06612. In the circular section, it is constant until the superelevation decreases by approximately 10 meters, and in the last section of the circular curve, this factor starts to decrease. In the last section of the path that is

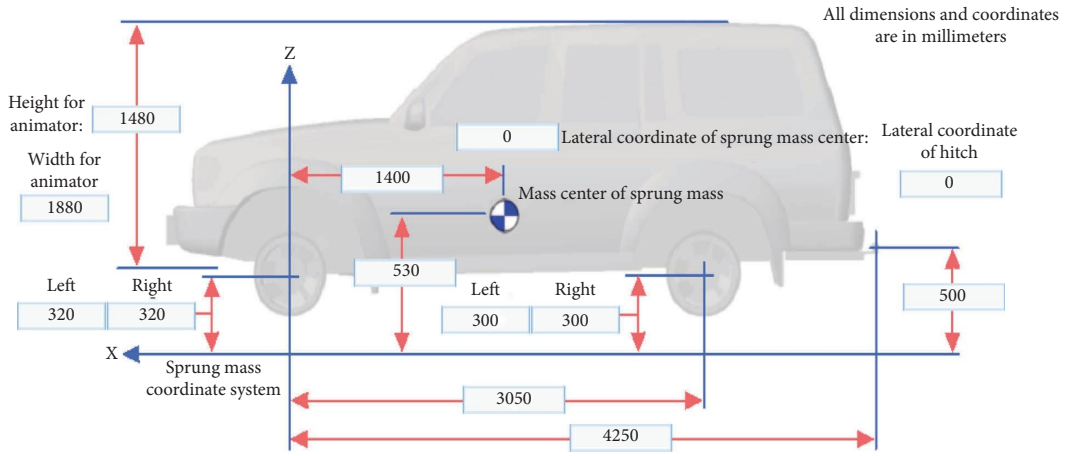

Figure 3: Dimensions and mass of E-class sedan.

Figure 4: E-class SUV.

Table 3: Specifications of E-class SUV.

Parameter	Value
Length	4220 mm
Width	1875 mm
Height	1800 mm
Wheels distance	2950 mm
Wheel center height from the ground	385 mm
Mass center height	719 mm
Weight	1592 kg

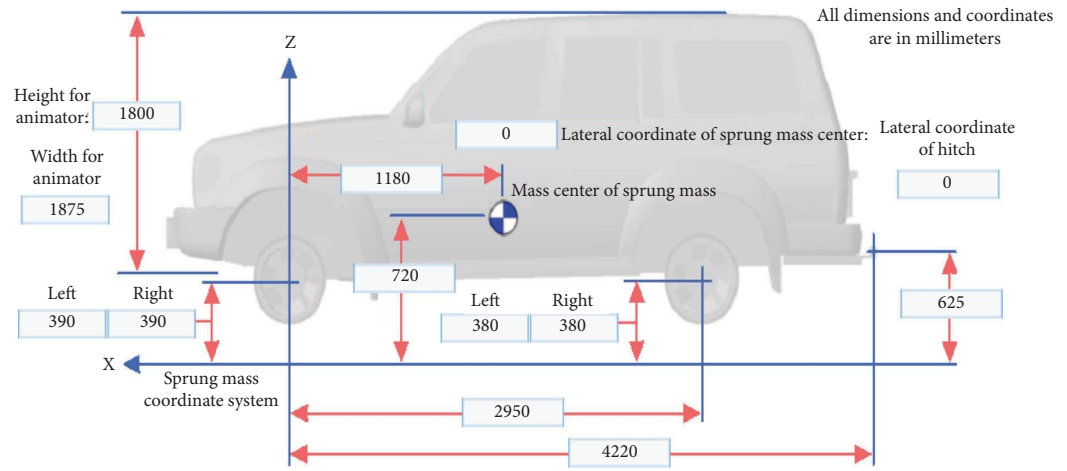

Figure 5: Dimensions and mass of E-class SUV.

Figure 6: Two-axle truck.

Table 4: Specifications of E-class SUV.

Parameter	Value (driver's room)	Value (cargo)
Length	—	3000 mm
Width	2438 mm	2000 mm
Height	3200 mm	1000 mm
Wheels distance	—	—
Wheel center height from the ground	—	—
Mass center height	1173 mm	1800 mm
Weight	4457 kg	6789 kg

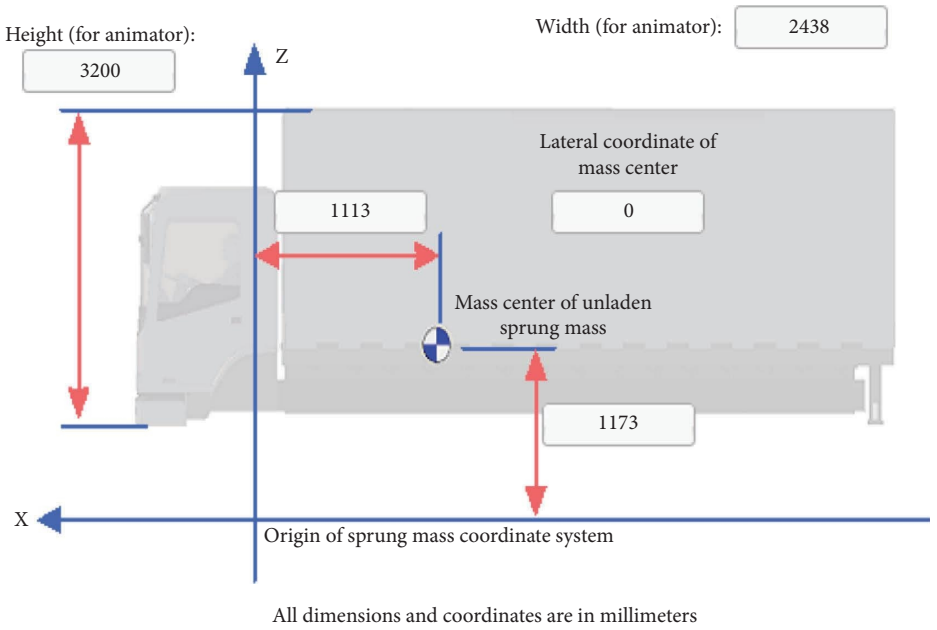

Figure 7: Dimensions and mass of two-axle truck.

a tangent path, reducing the side friction factor continues until the minimum side friction factor, which is equal to −0.044154. After that, the side friction factor increases until the end point of employing superelevation and remains constant until the path ends.

From Figure 13, which indicates the side friction factor in spiral horizontal curves along the path, it can be seen that the side friction factor in different sections of the path is split into the tangent, spiral, circular curve, spiral, and tangent. In the tangent path, the side friction factor is constant for 18 meters from the path start to the spiral start and increases after that. This factor in the spiral section continues to increase and also changes in three phases in the circular curve. In the first phase, this factor continues to increase until a maximum of 0.06564. In the second phase, the side friction factor is constant, and in the third phase, this factor starts to decrease. After the circular curve, in the spiral section, the side friction factor

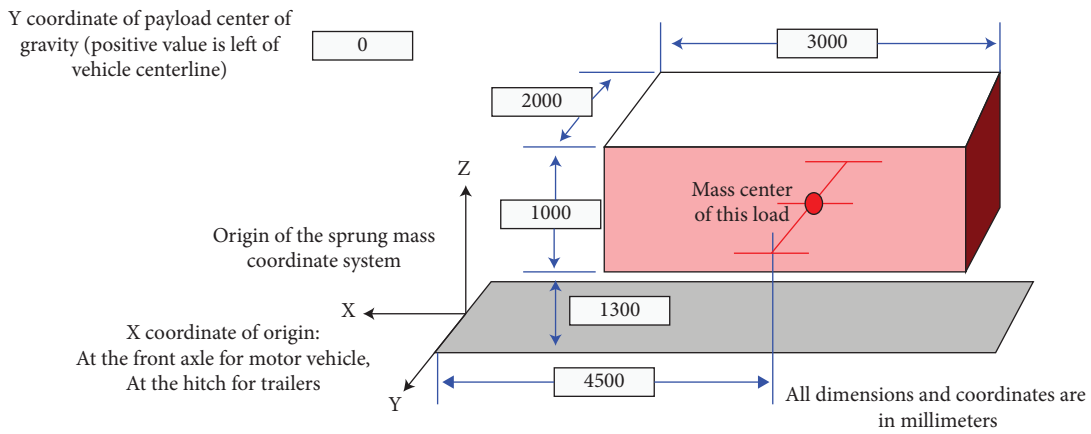

Figure 8: Two-axle truck cargo specifications.

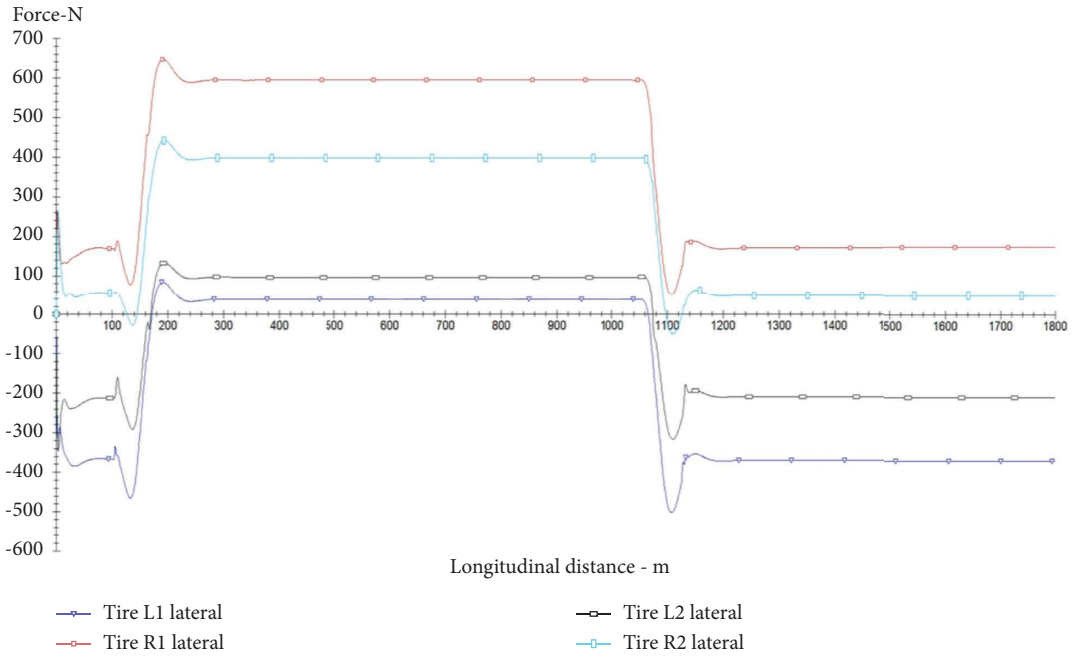

Figure 9: Diagram of the lateral force on the wheels of vehicles.

continues to decrease, and eventually, the side friction factor remains constant in the tangent path.

Figure 14 shows the side friction factor in a simple horizontal curve with a radius equal to the maximum radius of spiral use (fy (1 R) C.C) and the side friction factor in a spiral horizontal curve with a radius equal to the maximum radius of spiral use (fy (1 R) C.S). From this figure, it is concluded that in a simple horizontal curve, the maximum side friction factor is higher than the maximum side friction factor in a spiral horizontal curve. Also, the process of increasing this factor in the spiral curve takes place with a gentler slope.

According to Figure 15, R is the maximum radius of spiral use, and 0.7, 0.9, 1, 1.1, and 1.3 are curve radius change coefficients. From this figure, it can be seen that the smaller the radius of simple and spiral horizontal curves, the greater the side friction factor. Also, it is evident that the maximum side friction factors in all radii are greater in simple horizontal curves.

Table 5 indicates the difference between the maximum side friction factor at the speed of 100 km/h in simple and spiral horizontal curves. It is obvious from the table that the least difference of percentage compared to the simple curve occurs in the curve radius percentage of 90%.

Figure 16 illustrates a comparison of the maximum side friction factor versus speed at radii of 1.3 R, 1.1 R, R, 0.9 R, and 0.7 R for the truck in simple and spiral horizontal curves. As it is evident, by increasing the speed, the maximum side friction factor decreases. Also, the maximum amount of this factor in the speed range between 30 and 70 km/h of simple and spiral horizontal curves is almost equal; however, the maximum side friction factor in the speed range of 70 to

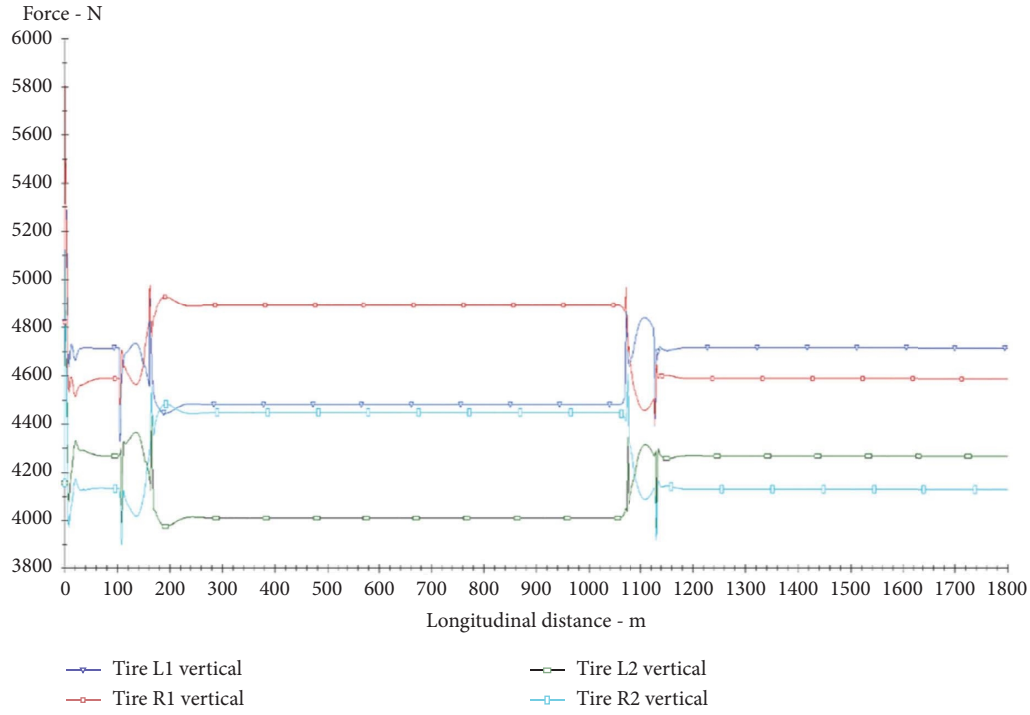

Figure 10: Diagram of the vertical force on the wheels of vehicles.

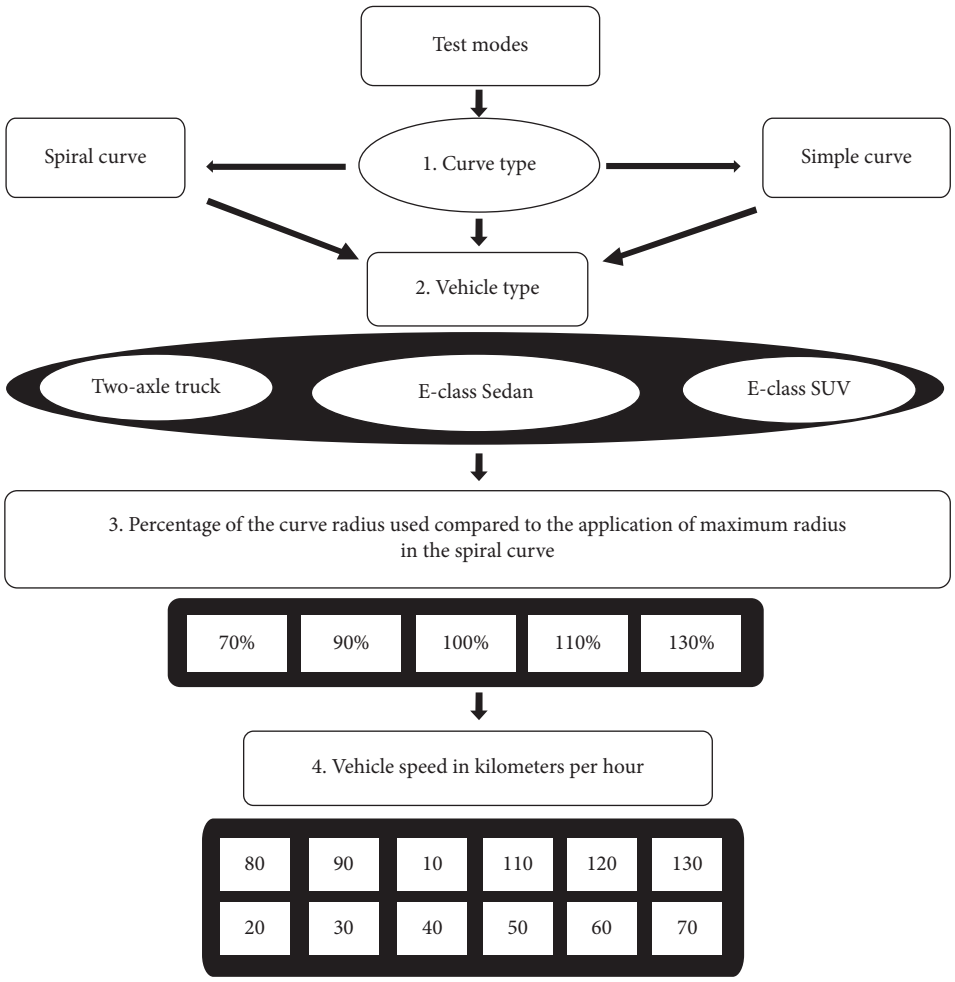

Figure 11: Flowchart of the tests presented in the research.

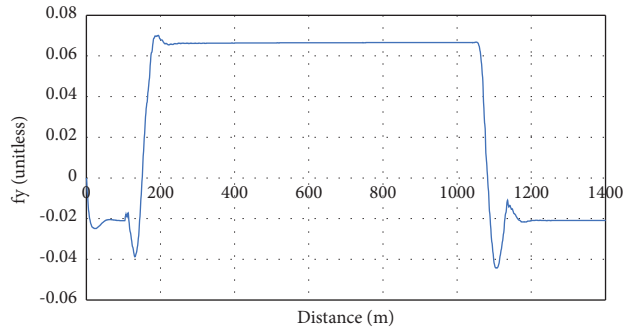

Figure 12: Side friction factor in simple horizontal curves along the path of a truck.

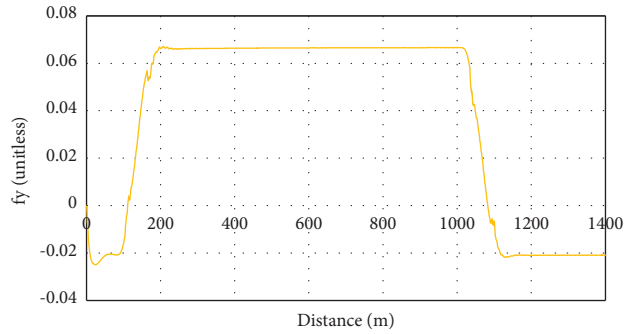

Figure 13: Side friction factor in spiral horizontal curves along the path of a truck.

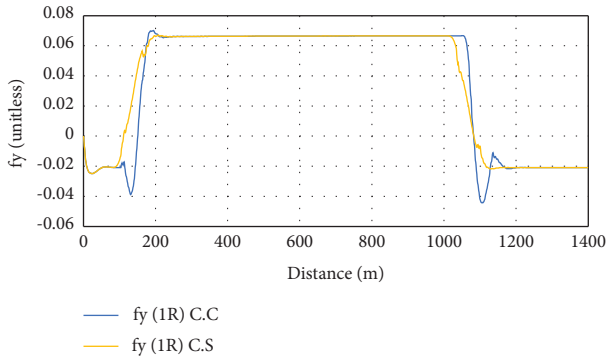

Figure 14: Comparison of side friction factors along the path between simple and spiral horizontal curves for a truck.

130 km/h in the simple curve is higher than that of the spiral curve.

4.1.2. Comparison between the Maximum Side Friction Factor Obtained with AASHTO Green Book for a Truck. In this section, the maximum side friction factor amounts for simple and spiral horizontal curves of different radii are compared with those recommended by AASHTO. Table 6 presents the maximum side friction factor amounts recommended by AASHTO.

Tables 7–11 show the comparison of the maximum side friction factor between the simple and spiral horizontal curves and AASHTO recommended values in the radii of 1.3, 1.1, 1, 0.9, and 0.7 times the maximum radius of spiral use. As can be seen from Tables 7–10, the maximum amount in the simple and spiral horizontal curves is lower than the AASHTO recommended values. Table 11 also shows that the maximum side friction factor in a simple curve at speeds 130, 120, and 110 km/h is higher than the amounts recommended by AASHTO, but speeds that are not mentioned are lower than recommended values. Also, the maximum amount in the spiral curve at speeds of 130 and 120 km/h is higher compared to those recommended by AASHTO; however, speeds that are not aforementioned are lower than the recommended values. It can also be concluded from the tables that the maximum side friction factor of the spiral horizontal curve at all speeds is less than the simple horizontal curve. Therefore, as explained, the spiral horizontal curve is better and safer compared to the simple one for the two-axle truck based on the side friction factor.

4.2. Side Friction Factor Diagrams for Sedan

4.2.1. Side Friction Factor in the Path. Figure 17 displays a comparison of the maximum side friction factor versus the speed in radii of 1.3 R, 1.1 R, R, 0.9 R, and 0.7 R for sedan in simple and spiral horizontal curves. According to Figure 17(a), it can be said that by increasing speeds, the maximum side friction factor increases. However, the maximum side friction factor at different speeds in Figure 17(b) for a radius of 1.1 R shows a variable behavior. Also, according to Figures 17(c) and 17(d), the maximum side friction factor is almost constant with increasing speed in the simple horizontal curve, and in the spiral horizontal curve, the maximum side friction factor decreases with increasing speed. But, as it is clear from Figure 17(e), the higher the speed, the maximum side friction factor increases in the simple horizontal curve, and it is almost constant in the spiral horizontal curve with an increasing speed. Also, as the figures show, the maximum side friction factor is almost equal in simple and spiral horizontal curves for Figures 17(a)–17(e) in the speed range between 30 and 40 km/h and for Figures 17(c) and 17(d) in the speed range between 20 and 40 km/h, and for all these radii, in the speed range of 40 to 130 km/h, the maximum side friction factor in the simple horizontal curve is higher than that in the spiral horizontal curve.

4.2.2. Comparison between the Maximum Side Friction Factor Obtained with AASHTO Green Book for Sedan. Tables 12–16 show the comparison of the maximum side friction factor between AASHTO recommended values and the simple and spiral horizontal curves for sedan in the radii of 1.3, 1.1, 1, 0.9, and 0.7 times the maximum radius of using spiral. Tables 12–15 show that the maximum side friction factor in these curves (except for the maximum side friction factor in the simple horizontal curve at 130 km/h speed in Table 15) is less than the amounts recommended by AASHTO. On the other hand, as can be seen from Table 16, the maximum side friction factor in a simple horizontal

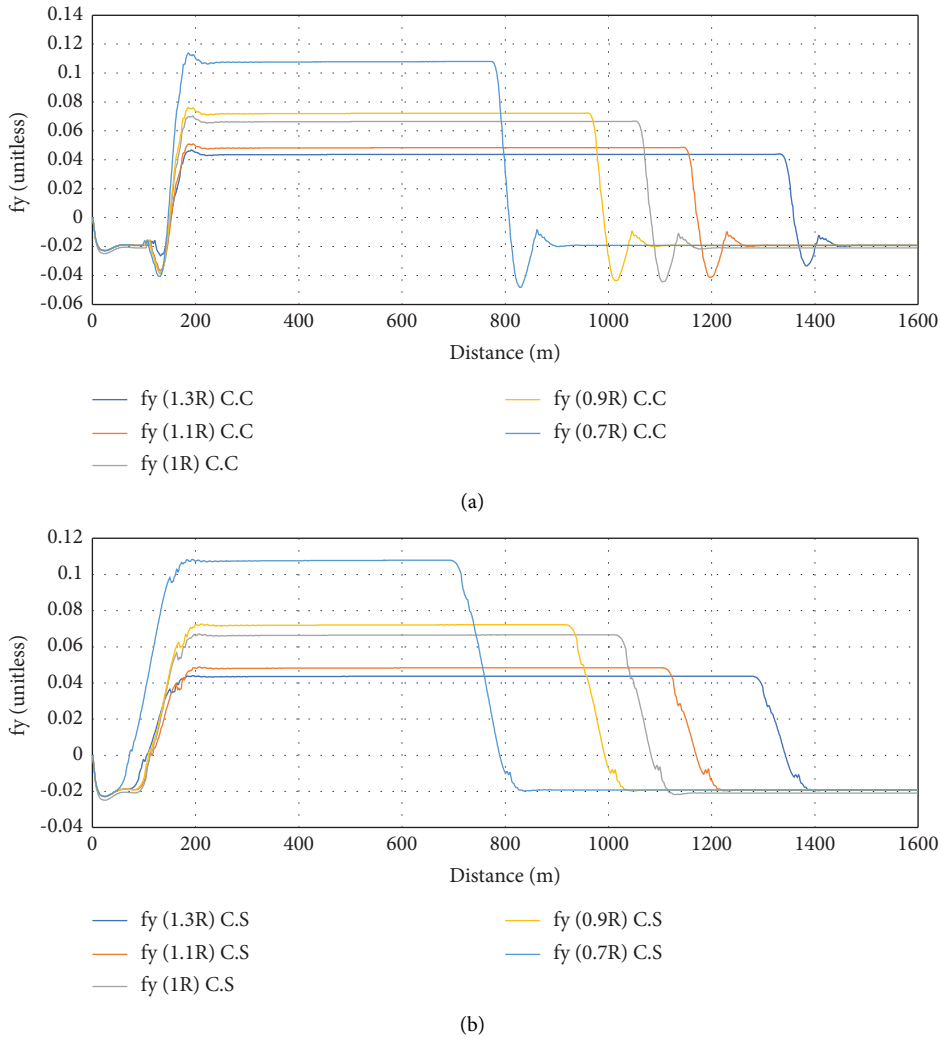

Figure 15: Comparison of side friction factors for the truck between different radii of horizontal curves: (a) simple and (b) spiral.

Table 5: The difference of percentage between the maximum side friction factor in simple and spiral horizontal curves for the truck.

Curve radius percentage	Simple curve	Spiral curve	Percentage difference compared to the simple curve
130	0.045621314	0.04510878	1.123453273
110	0.058097401	0.057756158	0.587365094
100	0.066129416	0.065648924	0.726592785
90	0.077668571	0.077365609	0.390070747
70	0.112757634	0.112150355	0.538570502

curve at speeds of 130, 120, 110, and 100 km/h and in a spiral horizontal curve at speeds of 130, 120, and 110 km/h is higher than the recommended values. However, the speeds not mentioned before are lower in comparison with AASHTO recommended values. Moreover, the maximum side friction factor in the spiral horizontal curve at all speeds is less than that in the simple horizontal curve. Therefore, it can be concluded that the spiral horizontal curve is better and safer in comparison with the simple horizontal curve for sedans based on the side friction factor.

4.3. Side Friction Factor Diagrams for SUV

4.3.1. Side Friction Factor in the Path. Figure 18 illustrates a comparison of the maximum side friction factor versus the speed at radii 1.3 R, 1.1 R, R, 0.9 R, and 0.7 R for SUV in simple and spiral horizontal curves. According to Figure 18(a), it can be said that by increasing speeds, the maximum side friction factor increases in the simple horizontal curve; however, the increase in the maximum side friction factor is very low in the spiral horizontal curve. Also, in Figure 18(b), the maximum side friction factor at different speeds for 1.1 R radius shows a

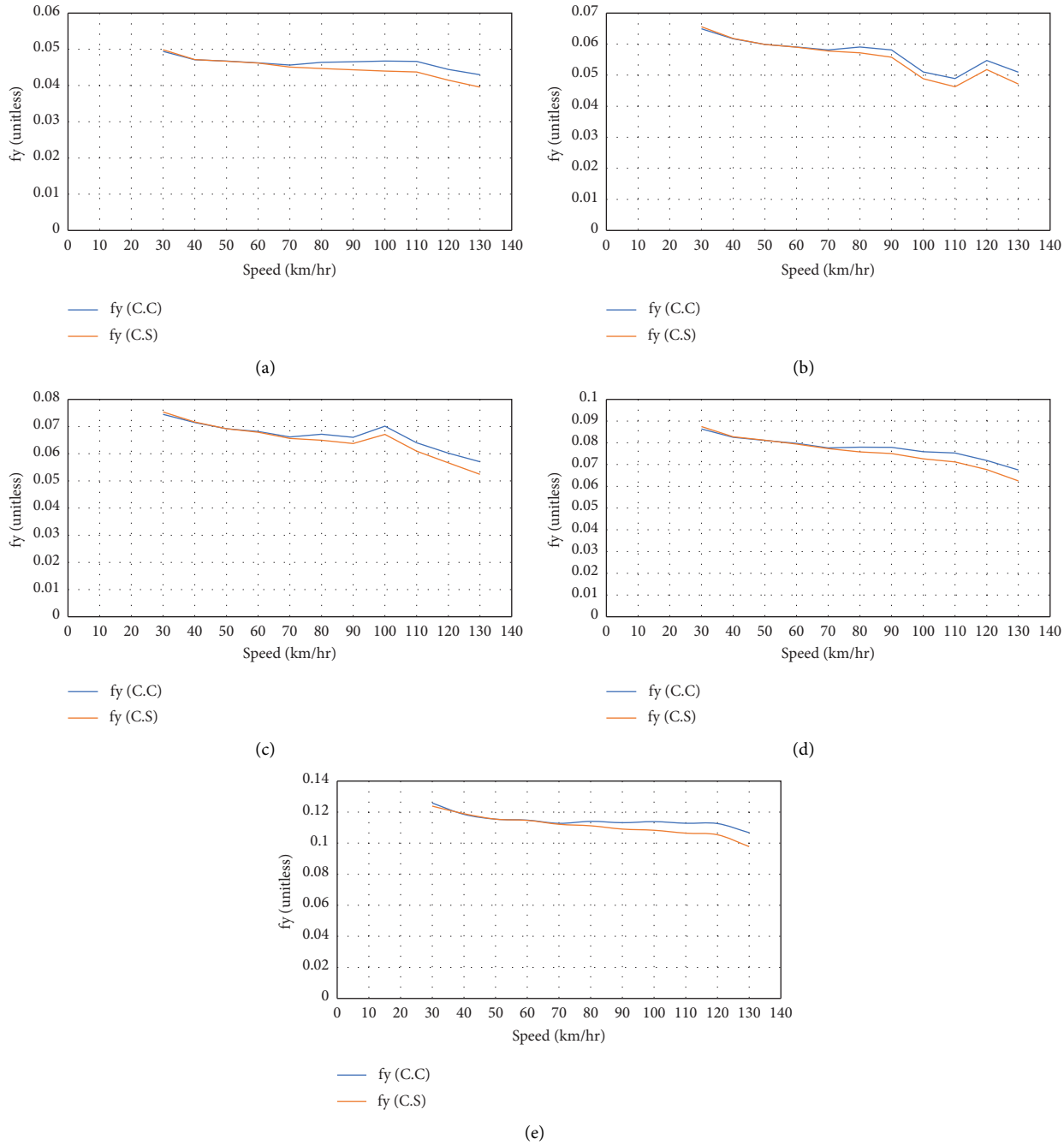

Figure 16: Comparison between the maximum side friction factor of a truck in simple and spiral horizontal curves versus the speed in the radii: (a) 1.3 R, (b) 1.1 R, (c) R, (d) 0.9 R, and (e) 0.7 R.

Table 6: Maximum side friction factor amounts recommended by AASHTO.

Speed (km/h)	AASHTO recommended values	Speed (km/h)	AASHTO recommended values
130	0.08	70	0.15
120	0.09	60	0.17
110	0.11	50	0.19
100	0.12	40	0.23
90	0.13	30	0.28
80	0.14	20	0.35

Table 7: Comparison of the maximum side friction factor for a truck between simple and spiral horizontal curves and AASHTO recommended values at a radius of 1.3 R.

Speed (km/h)	Maximum side friction factor		
	Simple horizontal curve	AASHTO	Spiral horizontal curve
130	0.042993	0.08	0.03956
120	0.044423	0.09	0.041446
110	0.046637	0.11	0.043708
100	0.046758	0.12	0.043992
90	0.046542	0.13	0.044351
80	0.046399	0.14	0.04467
70	0.045621	0.15	0.045109
60	0.046263	0.17	0.046206
50	0.046727	0.19	0.046676
40	0.047113	0.23	0.047137
30	0.049415	0.28	0.049873
20	0.062086	0.35	0.059058

Table 8: Comparison of the maximum side friction factor for a truck between simple and spiral horizontal curves and AASHTO recommended values at a radius of 1.1 R.

Speed (km/h)	Maximum side friction factor		
	Simple horizontal curve	AASHTO	Spiral horizontal curve
130	0.05099	0.08	0.047159
120	0.054744	0.09	0.05178
110	0.048893	0.11	0.046288
100	0.05102	0.12	0.04886
90	0.058118	0.13	0.055778
80	0.059087	0.14	0.057199
70	0.058097	0.15	0.057756
60	0.059071	0.17	0.059028
50	0.059914	0.19	0.059879
40	0.061713	0.23	0.061852
30	0.064911	0.28	0.065582
20	0.080482	0.35	0.076659

Table 9: Comparison of the maximum side friction factor for a truck between simple and spiral horizontal curves and AASHTO recommended values at a radius of 1 R.

Speed (km/h)	Maximum side friction factor		
	Simple horizontal curve	AASHTO	Spiral horizontal curve
130	0.057053	0.08	0.052393
120	0.060151	0.09	0.056654
110	0.064027	0.11	0.06094
100	0.070139	0.12	0.067084
90	0.066053	0.13	0.063713
80	0.06713	0.14	0.064915
70	0.066129	0.15	0.065649
60	0.068171	0.17	0.067893
50	0.069202	0.19	0.069175
40	0.071484	0.23	0.071678
30	0.074446	0.28	0.075332
20	0.091422	0.35	0.088144

variable behavior. According to Figures 18(c)–18(e), it can be said that by increasing speeds, the maximum side friction factor increases in the simple curve and decreases in the spiral curve. On the other hand, as can be seen in the figure, the maximum side friction factor in the simple curve is higher than that in the spiral curve.

Table 10: Comparison of the maximum side friction factor for a truck between simple and spiral horizontal curves and AASHTO recommended values at a radius of 0.9 R.

Speed (km/h)	Maximum side friction factor		
	Simple horizontal curve	AASHTO	Spiral horizontal curve
130	0.067495	0.08	0.062516
120	0.071875	0.09	0.067692
110	0.075276	0.11	0.071228
100	0.075872	0.12	0.072608
90	0.077913	0.13	0.075095
80	0.07797	0.14	0.075853
70	0.077669	0.15	0.077366
60	0.079738	0.17	0.079429
50	0.081137	0.19	0.081171
40	0.082518	0.23	0.082741
30	0.086407	0.28	0.08747
20	0.105456	0.35	0.098039

Table 11: Comparison of the maximum side friction factor for a truck between simple and spiral horizontal curves and AASHTO recommended values at a radius of 0.7 R.

Speed (km/h)	Maximum side friction factor		
	Simple horizontal curve	AASHTO	Spiral horizontal curve
130	0.106729	0.08	0.097789
120	0.112617	0.09	0.105401
110	0.112807	0.11	0.106434
100	0.113855	0.12	0.1083
90	0.11317	0.13	0.109063
80	0.114039	0.14	0.111185
70	0.112758	0.15	0.11215
60	0.114821	0.17	0.114676
50	0.115452	0.19	0.115461
40	0.118561	0.23	0.118967
30	0.125832	0.28	0.123854
20		0.35	

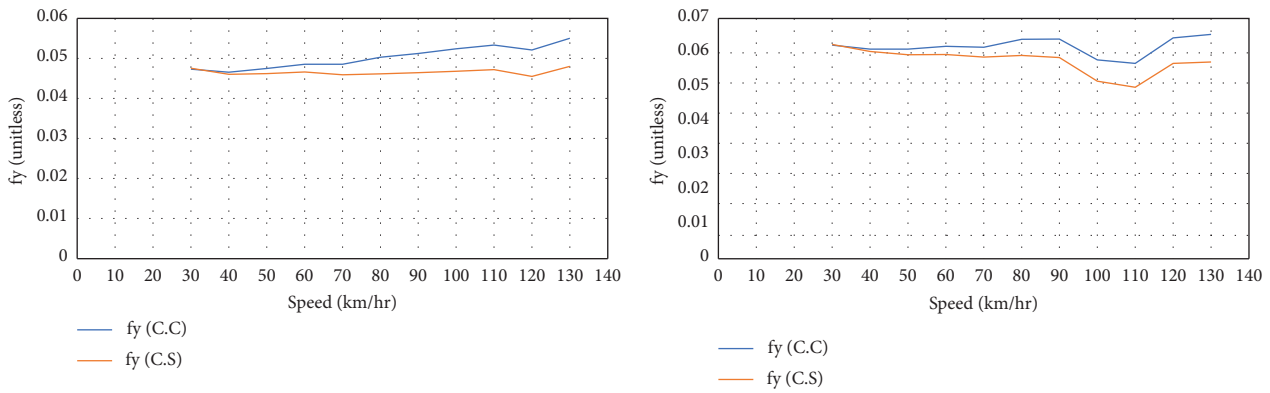

(a) (b)

Figure 17: Continued.

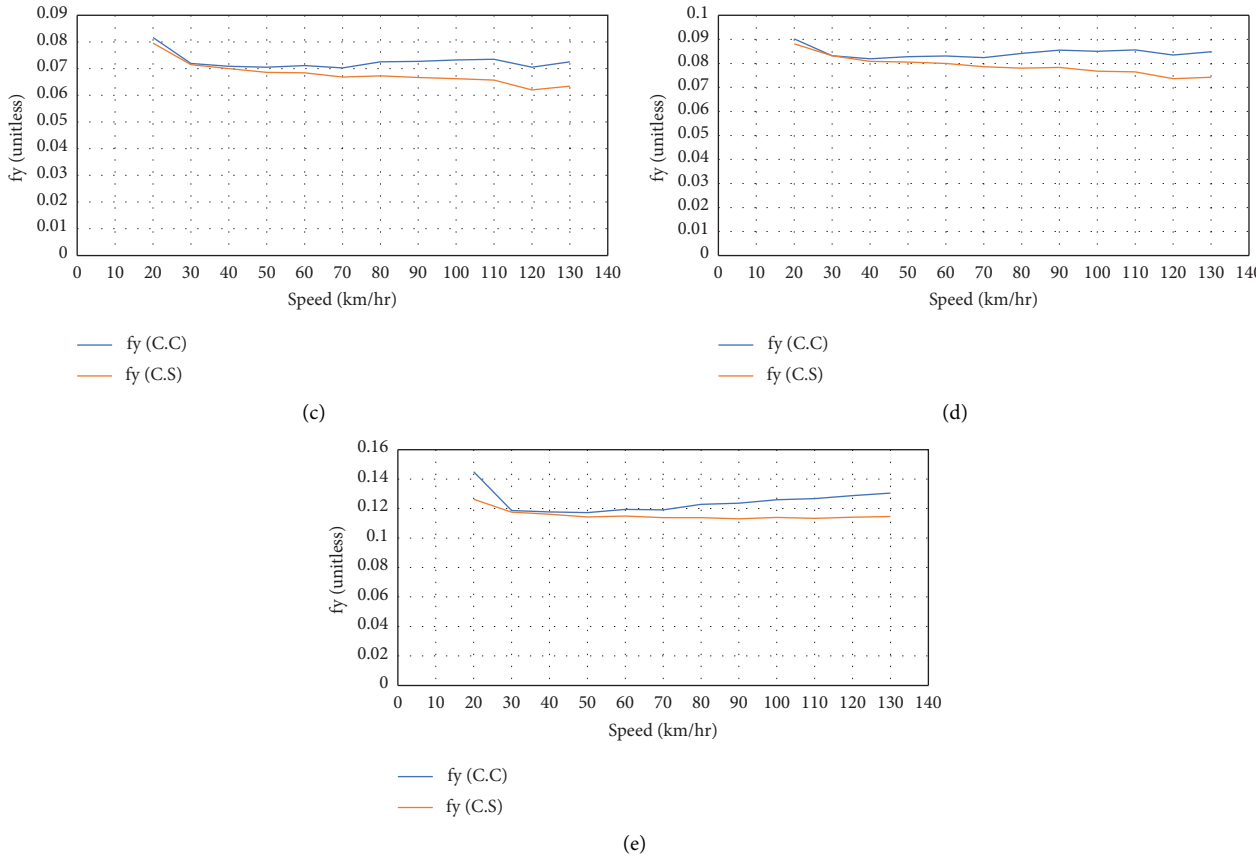

Figure 17: Comparison of the maximum side friction factor for sedan in simple and spiral horizontal curves versus the speed in the radii: (a) 1.3 R, (b) 1.1 R, (c) R, (d) 0.9 R, and (e) 0.7 R.

Table 12: Comparison of the maximum side friction factor between simple and spiral horizontal curves and AASHTO recommended values for sedan at a radius of 1.3 R.

Speed (km/h)	Maximum side friction factor		
	Simple horizontal curve	AASHTO	Spiral horizontal curve
130	0.054992	0.08	0.047979
120	0.05211	0.09	0.045465
110	0.053312	0.11	0.047211
100	0.052363	0.12	0.046791
90	0.051206	0.13	0.046421
80	0.050306	0.14	0.046115
70	0.048501	0.15	0.045918
60	0.048553	0.17	0.046628
50	0.047504	0.19	0.046216
40	0.046567	0.23	0.046013
30	0.047318	0.28	0.047522
20	0.05557	0.35	0.054377

4.3.2. Comparison between the Maximum Side Friction Factor Obtained with AASHTO Green Book for SUV. Tables 17–21 show the comparison of the maximum side friction factor between AASHTO recommended values and simple and spiral horizontal curves in the radii of 1.3, 1.1, 1, 0.9, and 0.7 times the maximum radius of using spiral for SUV. As can be seen from Tables 17–20, the maximum side friction factor (except for that in the simple curve at 130 km/h speed and a radius of 0.9 R) is lower in the simple and spiral horizontal curves compared to AASHTO recommended values. On the other hand, as can be seen from Table 21, the maximum side friction factor in a simple curve at speeds of 130, 120, 110, and 100 km/h and in a spiral horizontal curve at speeds of 130, 120, and 110 km/h is

Table 13: Comparison of the maximum side friction factor between simple and spiral horizontal curves and AASHTO recommended values for sedan at a radius of 1.1 R.

Speed (km/h)	Maximum side friction factor		
	Simple horizontal curve	AASHTO	Spiral horizontal curve
130	0.065338	0.08	0.057285
120	0.064337	0.09	0.056925
110	0.05688	0.11	0.049975
100	0.057911	0.12	0.051731
90	0.064002	0.13	0.0586
80	0.063897	0.14	0.059185
70	0.061599	0.15	0.058758
60	0.061887	0.17	0.059493
50	0.061082	0.19	0.059428
40	0.061083	0.23	0.06038
30	0.062224	0.28	0.062415
20	0.071937	0.35	0.070409

Table 14: Comparison of the maximum side friction factor between simple and spiral horizontal curves and AASHTO recommended values for sedan at a radius of 1 R.

Speed (km/h)	Maximum side friction factor		
	Simple horizontal curve	AASHTO	Spiral horizontal curve
130	0.072557	0.08	0.063385
120	0.070512	0.09	0.062017
110	0.073521	0.11	0.065656
100	0.073259	0.12	0.066195
90	0.072682	0.13	0.066686
80	0.072497	0.14	0.067281
70	0.070239	0.15	0.066793
60	0.071103	0.17	0.068401
50	0.070533	0.19	0.068605
40	0.070896	0.23	0.069988
30	0.071907	0.28	0.071494
20	0.08162	0.35	0.079566

Table 15: Comparison of the maximum side friction factor between simple and spiral horizontal curves and AASHTO recommended values for sedan at a radius of 0.9 R.

Speed (km/h)	Maximum side friction factor		
	Simple horizontal curve	AASHTO	Spiral horizontal curve
130	0.084799	0.08	0.0742
120	0.083441	0.09	0.073644
110	0.08558	0.11	0.076465
100	0.084998	0.12	0.076775
90	0.085503	0.13	0.078343
80	0.084194	0.14	0.078041
70	0.082385	0.15	0.078632
60	0.083079	0.17	0.079968
50	0.082779	0.19	0.080501
40	0.081873	0.23	0.080831
30	0.083155	0.28	0.083191
20	0.090177	0.35	0.088139

Table 16: Comparison of the maximum side friction factor between simple and spiral horizontal curves and AASHTO recommended values for sedan at a radius of 0.7 R.

Speed (km/h)	Maximum side friction factor		
	Simple horizontal curve	AASHTO	Spiral horizontal curve
130	0.130459	0.08	0.114606
120	0.128785	0.09	0.114125
110	0.126819	0.11	0.113415
100	0.126004	0.12	0.11394
90	0.12359	0.13	0.113047
80	0.122894	0.14	0.113895
70	0.119084	0.15	0.113796
60	0.119475	0.17	0.114979
50	0.117313	0.19	0.11432
40	0.117792	0.23	0.116127
30	0.118728	0.28	0.117493
20	0.145012	0.35	0.12633

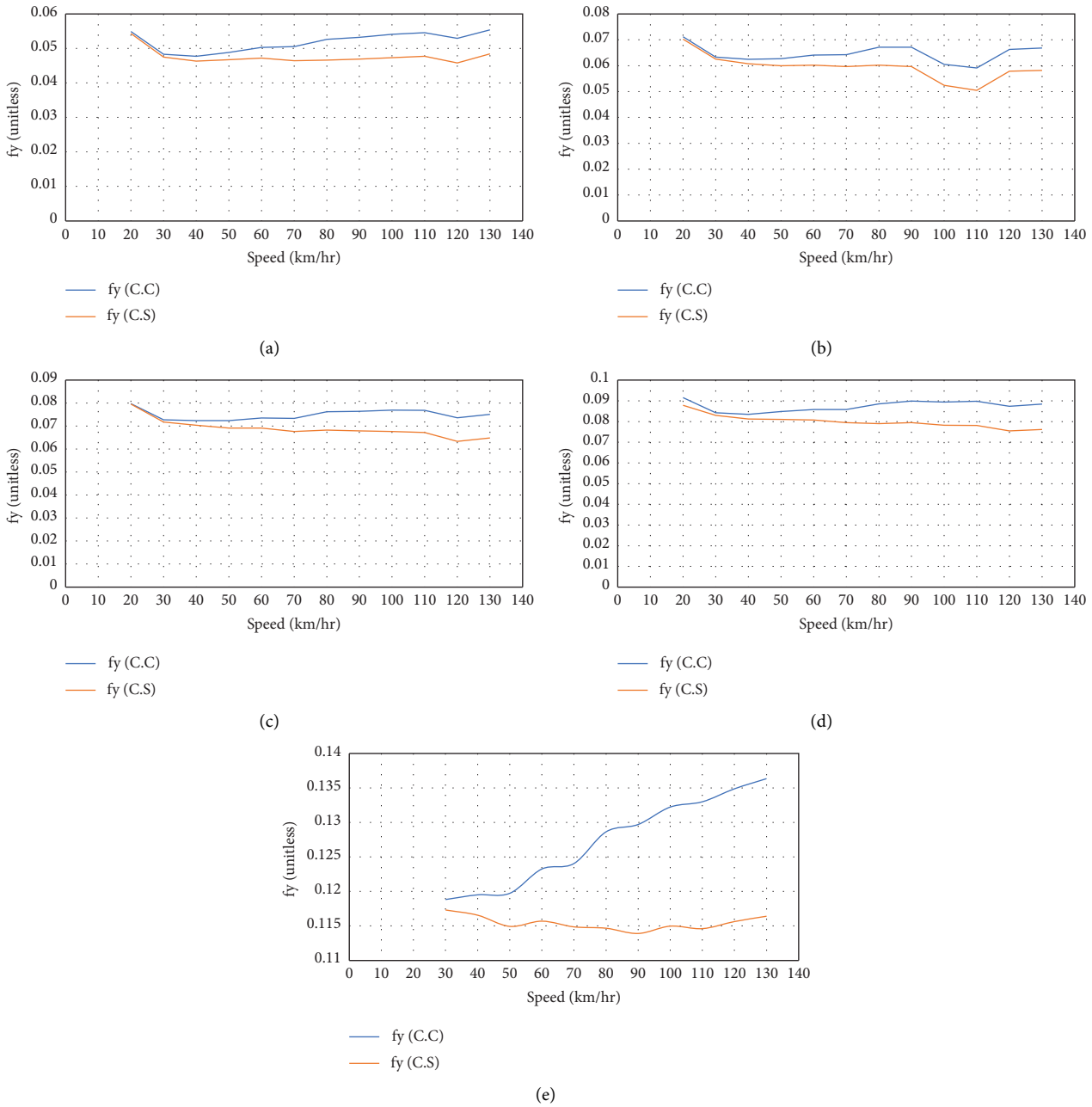

Figure 18: Comparison of the maximum side friction factor for SUV versus the speed in simple and spiral horizontal curves in the radii: (a) 1.3 R, (b) 1.1 R, (c) R, (d) 0.9 R, and (e) 0.7 R.

Table 17: Comparison of the maximum side friction factor for SUV between simple and spiral horizontal curves and AASHTO recommended values at a radius of 1.3 R.

Speed (km/h)	Maximum side friction factor		
	Simple horizontal curve	AASHTO	Spiral horizontal curve
130	0.055338	0.08	0.048425
120	0.052897	0.09	0.045805
110	0.054575	0.11	0.047714
100	0.05406	0.12	0.047297
90	0.053231	0.13	0.046906
80	0.052644	0.14	0.046597
70	0.050502	0.15	0.046434
60	0.05028	0.17	0.047183
50	0.048804	0.19	0.046706
40	0.047704	0.23	0.046334
30	0.04829	0.28	0.047486
20	0.054872	0.35	0.054326

Table 18: Comparison of the maximum side friction factor for SUV between simple and spiral horizontal curves and AASHTO recommended values at a radius of 1.1 R.

Speed (km/h)	Maximum side friction factor		
	Simple horizontal curve	AASHTO	Simple horizontal curve
130	0.066845	0.08	0.058178
120	0.066249	0.09	0.057885
110	0.059069	0.11	0.050488
100	0.060534	0.12	0.052404
90	0.067129	0.13	0.059683
80	0.067126	0.14	0.060171
70	0.064238	0.15	0.059618
60	0.064058	0.17	0.060159
50	0.062702	0.19	0.059952
40	0.062442	0.23	0.06072
30	0.063292	0.28	0.062507
20	0.07121	0.35	0.070234

Table 19: Comparison of the maximum side friction factor for SUV between simple and spiral horizontal curves and AASHTO recommended values at a radius of 1 R.

Speed (km/h)	Maximum side friction factor		
	Simple horizontal curve	AASHTO	Simple horizontal curve
130	0.075071	0.08	0.064775
120	0.073543	0.09	0.063362
110	0.076854	0.11	0.067177
100	0.076898	0.12	0.067586
90	0.076385	0.13	0.067884
80	0.07619	0.14	0.068262
70	0.073289	0.15	0.067615
60	0.073488	0.17	0.069085
50	0.072313	0.19	0.069145
40	0.072321	0.23	0.070381
30	0.072739	0.28	0.071701
20	0.079673	0.35	0.079503

higher than the recommended values, but the aforementioned speeds are not less compared to AASHTO recommended values. In addition, the maximum side friction factor of the spiral curve at all speeds is less than the simple curve. Therefore, it can be concluded that the spiral horizontal curve is better and safer compared to the

Table 20: Comparison of the maximum side friction factor for SUV between simple and spiral horizontal curves and AASHTO recommended values at a radius of 0.9 R.

Speed (km/h)	Maximum side friction factor		
	Simple horizontal curve	AASHTO	Simple horizontal curve
130	0.088455	0.08	0.076141
120	0.087407	0.09	0.075434
110	0.0898	0.11	0.078121
100	0.089408	0.12	0.078161
90	0.089893	0.13	0.079504
80	0.088482	0.14	0.078979
70	0.085849	0.15	0.079516
60	0.085836	0.17	0.080699
50	0.084866	0.19	0.081053
40	0.083464	0.23	0.081228
30	0.084277	0.28	0.082996
20	0.091504	0.35	0.087893

Table 21: Comparison of the maximum side friction factor for SUV between simple and spiral horizontal curves and AASHTO recommended values at a radius of 0.7 R.

Speed (km/h)	Maximum side friction factor		
	Simple horizontal curve	AASHTO	Simple horizontal curve
130	0.136344	0.08	0.116406
120	0.134872	0.09	0.115632
110	0.132991	0.11	0.114606
100	0.132226	0.12	0.114969
90	0.129702	0.13	0.113907
80	0.128636	0.14	0.114667
70	0.12404	0.15	0.114863
60	0.12325	0.17	0.11569
50	0.119727	0.19	0.114935
40	0.119506	0.23	0.116555
30	0.118826	0.28	0.11731
20	0.145187	0.35	0.126274

simple horizontal curve for SUV based on the side friction factor.

5. Conclusions

In this study, the safety of simple and spiral horizontal curves was compared based on the side friction factor using vehicle dynamic simulation. For this aim, CarSim and TruckSim simulation softwares were applied to model the vehicle behavior in simple and spiral horizontal curves, and finally, the simulation outputs were obtained and drawn. The results showed the following:

(i) In all studied vehicles, the maximum side friction factor in the simple horizontal curve is higher than that in the spiral horizontal curve. Also, the process of increasing the side friction factor in the spiral horizontal curve takes place with a gentler slope.

(ii) For trucks, in all radii percentages except for 70% radius, the maximum side friction factor is lower than AASHTO recommended values in simple and spiral horizontal curves, showing that the spiral horizontal curve is better and safer than the simple horizontal curve in terms of side friction factor.

(iii) For trucks at a radius of 70%, the maximum side friction factor in a simple horizontal curve is higher than the amounts recommended by AASHTO at speeds of 130, 120, and 110 km/h and in the spiral horizontal curve at speeds of 130 and 120 km/h, but not mentioned speeds are lower than the recommended values.

(iv) For sedans and SUVs at all radii percentages except for 90% and 70% radius, the maximum side friction factor is lower than the AASHTO recommended values in simple and spiral horizontal curves, which indicates that the spiral curve is better than the simple one regarding this factor.

(v) For sedans and SUVs at a radius of 90%, the maximum side friction factor at all speeds in simple and spiral horizontal curves, except for the maximum side friction factor in the simple curve at 130 km/h speed, is less compared to AASHTO's recommended amounts.

(vi) For sedans and SUVs at a radius of 70%, the maximum side friction factor at speeds of 130, 120, 110, and 100 km/h in a simple horizontal curve and at speeds of 130, 120, and 110 km/h in a spiral horizontal curve is higher in comparison with amounts recommended by AASHTO. However, not all of the aforementioned speeds are less than recommended.

(vii) Finally, according to the results, the spiral horizontal curve is better and safer than the simple horizontal curve in this study, according to the side friction factor.

For future research, it is recommended that the effects of some parameters, such as braking scenarios, on the side friction factor of vehicles be investigated. Moreover, other vehicle types can be included in the simulation, such as minibus, bus, 3-axle and 4-axle trucks, and station wagons. Various environmental factors, weather conditions, and shoulder types can also be incorporated into the presented dynamic simulation method in future studies. In addition, the effects of superelevation changes on the side friction factor can be investigated. Furthermore, if field tests are possible, it is recommended the results and outputs be improved by comparing the results obtained from field tests and simulations. Also, the economic aspect and geometric design of these curves according to the project condition can be examined in the future [26]. In addition, various statistical analyses, machine learning, and optimization methods are recommended for further investigation [27–34]. Pavement failures can endanger traffic safety, and various additives and nanomaterials can be taken into account in this regard, which can be examined in a field investigation that is in line with this study [35–40]. Simulation devices and vehicles can also be adopted in incorporation with the Internet of Things (IoT), vehicle-mounted equipment, and sensors to develop the potential of driver motion and physiological signal monitoring [41–45]. Various human factors may cause a driver to leave the travel lane and affect the occurrence of accidents, such as driver's fatigue and inattention, which can be investigated in future research studies [46, 47]. Since the transportation sector is the second largest contributor to CO_2 emissions, a study can also be performed to evaluate the impact of pollutants on safety in continuation of this study [48, 49].

Data Availability

The data used to support the findings of this study are available from the corresponding author upon request.

Conflicts of Interest

The authors declare that they have no conflicts of interest. In this study, Iranian governmental organizations have not been partners and sponsors, and this study is purely studious.

References

[1] A. Garcia and D. Pastor-Serrano, "Determination of minimum horizontal curve radius for safe stopping sight distance of vehicles overpassing truck platoons," *Computer-Aided Civil and Infrastructure Engineering*, vol. 37, no. 5, pp. 539–557, 2022.

[2] M. Chakraborty and T. J. Gates, "Relationship between Horizontal Curve Density and Safety Performance on Rural Two-Lane Road Segments by Road Jurisdiction and Surface Type," in *Proceedings of the Transportation Research Board 100th Annual Meeting*, Washington, DC, USA, January 2021.

[3] B. Maljković and D. Cvitanić, "Improved horizontal curve design consistency approach using steady-state bicycle model combined with realistic speeds and path radii," *Journal of Transportation Engineering, Part A: Systems*, vol. 148, no. 9, Article ID 4022069, 2022.

[4] H. Pourkhani and A. A. Kordani, "Improving superelevation in spiral transitions based on lateral acceleration rate," in *Proceedings of the Institution Of Civil Engineers-Transport. 2021*, Thomas Telford Ltd, London, UK, July 2021.

[5] A. Ryan, E. Hennessy, C. Ai, W. Kwon, C. Fitzpatrick, and M. Knodler, "Driver performance at horizontal curves: bridging critical research gaps to increase safety," *Traffic Safety Research*, vol. 3, p. 14, 2022.

[6] J. Peng, L. Chu, T. Wang, and T. Fwa, "Analysis of vehicle skidding potential on horizontal curves," *Accident Analysis and Prevention*, vol. 152, Article ID 105960, 2021.

[7] J. S. Wood and S. Zhang, "Identification and calculation of horizontal curves for low-volume roadways using smartphone sensors," *Transportation Research Record*, vol. 2672, no. 39, pp. 1–10, 2018.

[8] A. F. Naser, "Analysis the effect of super-elevation on static and dynamic properties of horizontal curved concrete bridge by finite element," *Journal of Engineering Science and Technology*, vol. 16, no. 5, pp. 3669–3686, 2021.

[9] K. D. Jaiswal and E. S. Bhalerao, "Development of multisensory system for evaluation of horizontal curve super-elevation," *International Journal of Innovations in Engineering and Science*, vol. 40, 2018.

[10] J. Walker and J. Awange, "Transition curves and superelevation," in *Surveying for Civil and Mine Engineers*, pp. 230–259, Springer, New York, NY, USA, 2020.

[11] D. J. Torbic, E. T. Donnell, S. N. Brennan, A. Brown, M. K. O'Laughlin, and K. M. Bauer, "Superelevation design for sharp horizontal curves on steep grades," *Transportation Research Record*, vol. 2436, no. 1, pp. 81–91, 2014.

[12] C. H. Tan, *An Investigation of Comfortable Lateral Acceleration on Horizontal Curves*, The Pennsylvania State University, Pennsylvania, PA, USA, 2005.

[13] X. Wang, T. Wang, A. Tarko, and P. J. Tremont, "The influence of combined alignments on lateral acceleration on mountainous freeways: a driving simulator study," *Accident Analysis and Prevention*, vol. 76, pp. 110–117, 2015.

[14] J. A. Bonneson, "Superelevation distribution methods and transition designs," *Transportation Research Board*, vol. 439, 2000.

[15] A. M. Molan and A. A. Kordani, "Multi-body simulation modeling of vehicle skidding and roll over for horizontal curves on longitudinal grades," in *Proceedings of the 93rd Annual Meeting of TRB*, Washington, DC, USA, January 2014.

[16] A. A. Kordani, A. M. Molan, and S. Monajjem, "New formulas of side friction factor based on three-dimensional model in horizontal curves for various vehicles," in *T&DI Congress*

2014: Planes, Trains, and Automobiles, Orlando, Florida, FL, USA, 2014.

[17] A. A. Kordani and A. M. Molan, "The effect of combined horizontal curve and longitudinal grade on side friction factors," *KSCE Journal of Civil Engineering*, vol. 19, no. 1, pp. 303–310, 2015.

[18] A. A. Kordani, M. H. Sabbaghian, and B. T. Kallebasti, "Analyzing the influence of coinciding horizontal curves and vertical sag curves on side friction factor and lateral acceleration using simulation modeling," *TRR Journal*, 2015.

[19] A. Abdi Kordani, S. Javadi, and A. Fallah, "The effect of shoulder on safety of highways in horizontal curves: with focus on roll angle," *KSCE Journal of Civil Engineering*, vol. 22, no. 8, pp. 3153–3161, 2018.

[20] G. Qu, Y. He, X. Sun, and J. Tian, "Modeling of lateral stability of tractor-semitrailer on combined alignments of freeway," *Discrete Dynamics in Nature and Society*, vol. 2018, Article ID 8438921, 17 pages, 2018.

[21] A. Abdi, P. Aghamohammadi, R. Salehfard, V. Najafi, and M. Gilani, "Dynamic modelling of the effects of combined horizontal and vertical curves on side friction factor and lateral acceleration," in *IOP Conference Series: Materials Science and Engineering*, IOP Publishing, England, UK, 2019.

[22] A. S. Abdollahzadeh Nasiri, O. Rahmani, A. Abdi Kordani, N. Karballaeezadeh, and A. Mosavi, "Evaluation of safety in horizontal curves of roads using a multi-body dynamic simulation process," *International Journal of Environmental Research and Public Health*, vol. 17, no. 16, p. 5975, 2020.

[23] S. Javadi, I. Farzin, and A. Abdi, "Evaluation of the effect of road shoulder characteristics on dynamic parameters affecting on vehicle rollover in the joint of shoulder-roadway in horizontal curves," *Journal of Transportation Research*, vol. 18, no. 1, pp. 51–62, 2021.

[24] M. Moradi, A. Abdi Kordani, and M. Zarei, "New geometric design approach to reduce vehicle's speed in accident-prone downgrade highways using dynamic vehicle modeling," *Journal of Transportation Engineering, Part A: Systems*, vol. 147, no. 1, Article ID 4020149, 2021.

[25] M. Khanjari, A. Abdi Kordani, and M. Zarei, "Simulation and modelling of safety of roadways in reverse horizontal curves (RHCs): with focus on lateral acceleration," *Advances in Civil Engineering*, vol. 202212 pages, 2022.

[26] F. Faghihinejad, M. Mohammadi Fard, A. Roshanghalb, and P. Beigi, "A framework to assess the correlation between transportation infrastructure access and economics: evidence from Iran," *Mathematical Problems in Engineering*, vol. 2022, Article ID 8781686, 15 pages, 2022.

[27] Y. Li, P. Che, C. Liu, D. Wu, and Y. Du, "Cross-scene pavement distress detection by a novel transfer learning framework," *Computer-Aided Civil and Infrastructure Engineering*, vol. 36, no. 11, pp. 1398–1415, 2021.

[28] J. Wang, J. Tian, X. Zhang et al., "Control of time delay force feedback teleoperation system with finite time convergence," *Frontiers in Neurorobotics*, vol. 16, Article ID 877069, 2022.

[29] R. Li, X. Qian, C. Gong et al., "Simultaneous assessment of the whole eye biomechanics using ultrasonic elastography," *IEEE Transactions on Biomedical Engineering*, pp. 1–8, 2022.

[30] Y. Ban, M. Liu, P. Wu et al., "Depth estimation method for monocular camera defocus images in microscopic scenes," *Electronics*, vol. 11, no. 13, p. 2012, 2022.

[31] S. Li and Z. Liu, "Scheduling uniform machines with restricted assignment," *Mathematical Biosciences and Engineering*, vol. 19, no. 9, pp. 9697–9708, 2022.

[32] M. Liu, C. Li, Y. Zhang et al., "Analysis of grinding mechanics and improved grinding force model based on randomized grain geometric characteristics," *Chinese Journal of Aeronautics*, 2022.

[33] C. Luo, L. Wang, Y. Xie, and B. Chen, "A new conjugate gradient method for moving force identification of vehicle–bridge system," *Journal of Vibration Engineering and Technologies*, pp. 1–18, 2022.

[34] S. Lu, Y. Ban, X. Zhang et al., "Adaptive control of time delay teleoperation system with uncertain dynamics," *Frontiers in Neurorobotics*, vol. 16, Article ID 928863, 2022.

[35] V. Najafi Moghaddam Gilani, G. H. Hamedi, M. R. Esmaeeli, M. Habibzadeh, and M. Hosseinpour Eshkiknezhad, "Presentation of thermodynamic and dynamic modules methods to investigate the effect of nano hydrated lime on moisture damage of stone matrix asphalt," *Australian Journal of Civil Engineering*, vol. 2022, Article ID 2083404, 10 pages, 2022.

[36] X. Xiao, H. Zhang, Z. Li, and F. Chen, "Effect of temperature on the fatigue life assessment of suspension bridge steel deck welds under dynamic vehicle loading," *Mathematical Problems in Engineering*, vol. 2022, Article ID 7034588, 14 pages, 2022.

[37] W. Xu, C. Li, Y. Zhang et al., "Electrostatic atomization minimum quantity lubrication machining: from mechanism to application," *International Journal of Extreme Manufacturing*, vol. 4, no. 4, Article ID 42003, 2022.

[38] X. Cui, C. Li, Y. Zhang et al., "Comparative assessment of force, temperature, and wheel wear in sustainable grinding aerospace alloy using biolubricant," *Frontiers of Mechanical Engineering*, vol. 18, no. 1, pp. 3–33, 2023.

[39] Y. Yang, M. Yang, C. Li et al., "Machinability of ultrasonic vibration assisted micro-grinding in biological bone using nanolubricant," *Frontiers of Mechanical Engineering*, vol. 17, pp. 1–10, 2022.

[40] H. Zhang, L. Li, W. Ma, Y. Luo, Z. Li, and H. Kuai, "Effects of welding residual stresses on fatigue reliability assessment of a PC beam bridge with corrugated steel webs under dynamic vehicle loading," in *Structures*, Elsevier, Netherlands, Europe, 2022.

[41] Q. Zhang, C. Xin, F. Shen et al., "Human body iot systems based on the triboelectrification effect: energy harvesting, sensing, interfacing and communication," *Energy and Environmental Science*, vol. 15, 2022.

[42] S. Xiao, Y. Cao, G. Wu et al., "Influence of the distributed grounding layout for intercity trains on the 'train-rail'circumflux," *IEEE Transactions on Circuits and Systems II*, Express Briefs, 2022.

[43] Y. Du, B. Qin, C. Zhao, Y. Zhu, J. Cao, and Y. Ji, "A novel spatio-temporal synchronization method of roadside asynchronous MMW radar-camera for sensor fusion," *IEEE Transactions on Intelligent Transportation Systems*, vol. 23, no. 11, pp. 22278–22289, 2022.

[44] Y. Han, B. Wang, T. Guan et al., "Research on road environmental sense method of intelligent vehicle based on tracking check," *IEEE Transactions on Intelligent Transportation Systems*, vol. 24, no. 1, pp. 1261–1275, 2023.

[45] Y. Fang, H. Min, X. Wu, W. Wang, X. Zhao, and G. Mao, "On-ramp merging strategies of connected and automated vehicles considering communication delay," *IEEE Transactions on Intelligent Transportation Systems*, vol. 23, no. 9, pp. 15298–15312, 2022.

[46] J. Xu, X. Zhang, S. H. Park, and K. Guo, "The alleviation of perceptual blindness during driving in urban areas guided

by saccades recommendation," *IEEE Transactions on Intelligent Transportation Systems*, vol. 23, no. 9, pp. 16386–16396, 2022.

[47] J. Xu, S. H. Park, X. Zhang, and J. Hu, "The improvement of road driving safety guided by visual inattentional blindness," *IEEE Transactions on Intelligent Transportation Systems*, vol. 23, 2021.

[48] Y. Xiao, Y. Zhang, I. Kaku, R. Kang, and X. Pan, "Electric vehicle routing problem: a systematic review and a new comprehensive model with nonlinear energy recharging and consumption," *Renewable and Sustainable Energy Reviews*, vol. 151, Article ID 111567, 2021.

[49] Y. Xiao, X. Zuo, J. Huang, A. Konak, and Y. Xu, "The continuous pollution routing problem," *Applied Mathematics and Computation*, vol. 387, Article ID 125072, 2020.